Modeling preferential water flow and solute transport in unsaturated soil using the active region model

Feng Sheng

School of Environmental Science and Engineering, Sun Yat-Sen (Zhongshan) University, Guangzhou 510275, China.
School of Water Conservancy, Changsha University of Science and Technology, Changsha 410114, China.
E-mail: shengf.china@gmail.com

Kang Wang

State Key Lab. of Water Resources and Hydropower Engineering Science, Wuhan University, Wuhan 430072, China.
E-mail: wwangkang@163.com

Renduo Zhang (✉)

School of Environmental Science and Engineering, Sun Yat-Sen (Zhongshan) University, Guangzhou 510275, China.
E-mail: zhangrd@mail.sysu.edu.cn
Tel: +86 20 84110052; fax: +86 20 84110692

Huihai Liu

Earth Sciences Division, Lawrence Berkeley National Laboratory, Berkeley, CA 94720, USA.
E-mail: hhliu@lbl.gov

Modeling preferential water flow and solute transport in unsaturated soil using the active region model

Abstract Preferential flow and solute transport are common processes in the unsaturated soil, in which distributions of soil water content and solute concentrations are often characterized as fractal patterns. An active region model (ARM) was recently proposed to describe the preferential flow and transport patterns. In this study, ARM governing equations were derived to model the preferential soil water flow and solute transport processes. To evaluate the ARM equations, dye infiltration experiments were conducted, in which distributions of soil water content and Cl^- concentration were measured. Predicted results using the ARM and the mobile-immobile region model (MIM) were compared with the measured distributions of soil water content and Cl^- concentration. Although both the ARM and the MIM are two-region models, they are fundamental different in terms of treatments of the flow region. The models were evaluated based on the modeling efficiency (*ME*). The MIM provided relatively poor prediction results of the preferential flow and transport with negative *ME* values or positive *ME* values less than 0.4. On the contrary, predicted distributions of soil water content and Cl^- concentration using the ARM agreed reasonably well with the experimental data with *ME* values higher than 0.8. The results indicated that the ARM successfully

captured the macroscopic behavior of preferential flow and solute transport in the unsaturated soil.

Keywords Active region model · Preferential flow · Dye infiltration experiment · Mobile-immobile region model · Solute transport

Introduction

Preferential flow is a common phenomenon in the natural unsaturated soil (Heppell et al. 2000; Quisenberry et al. 1994). Preferential flow generally results in fast contaminant transport (Gjettermann et al. 1997; Morris and Mooney 2004; Reichenberger et al. 2002), and thus greatly increases the risk of groundwater contamination (Goulding et al. 2000; Jarvis 2000). Recent research results show that the preferential flow and solute transport in the unsaturated soil display fractal properties (e.g., Glass 1993; Öhrström et al. 2002; Persson et al. 2001; Smith and Zhang 2001). Liu et al. (2005) indicate that a key to successfully characterize preferential flow is to incorporate fractal or multi-fractal patterns into the model. Based on the fractal characteristics of preferential flow patterns, Liu et al. (2005) develop an active region model (ARM) to describe the macroscopic behavior of preferential flow and transport in the soil. The ARM is an extension of the active fracture model (AFM) developed for modeling unsaturated flow and transport in the fractured rock (Liu et al. 1998, 2003). Sheng et al. (2009) demonstrate that the ARM is able to capture the major features of the observed flow patterns under different infiltration conditions, and revealed that ARM parameter (γ) used for describing the flow heterogeneity may be scale independent within their experiment scales.

Similar to the mobile and immobile regions in the dual-domain model (Šimůnek et

al. 2003; van Genuchten and Wierenga 1976), in the ARM the whole flow region is divided into the active and inactive regions. However, the mobile region in the dual-domain model is fixed in the flow process, whereas the active region in the ARM is fractal and changeable, and the relative portion of the active region is expressed as a function of the soil water saturation in the flow region. The treatment of flow region in the ARM is consistent with the field observations (Larsson et al. 1999; Liu et al. 2005; van Dam et al. 1996; Sheng et al. 2009). While the previous studies on the ARM mainly focus on its constitutive relationship (Liu et al. 2005; Sheng et al. 2009), in this study, derivation and evaluation of ARM governing equations are presented for preferential water flow and solute transport in the unsaturated soil.

Dye infiltration experiments are being increasingly used to study the details of soil water flow from direct visualizations of flow paths (Morris and Mooney 2004). Owing to the high water solubility, limited toxicity, similar transport property to water, low adsorption in sand soil, and distinct visibility, food-grade dye pigment Brilliant Blue FCF has been considered as an excellent dye tracer for field experiments of soil water flow and solute transport (Flury and Flühler 1995; Kasteel et al. 2002; Ketelsen and Meyer-Windel 1999; Morris and Mooney 2004). The flow patterns can be characterized from the dye distributions for further quantitative research (Flury et al. 1994; Lipsius and Mooney 2006; Wang et al. 2006). Results from a well-controlled

dye-infiltration experiment were used to evaluate the ARM equations in this study.

The main objective of this paper was to derive the ARM governing equations for soil water flow and solute transport. Validity of the newly developed ARM governing equations was evaluated by comparing predicted results using the ARM with experimental distributions of soil water content and solute concentration, as well as with predicted results using the MIM.

The active region model

Constitutive relation

The ARM includes the following two basic assumptions (Liu et al. 2005):

1) The whole flow domain can be divided into the active region and the inactive region, and water flow and solute transport occur in the active region exclusively;

2) The active region displays fractal properties, and the portion of the active region is not fixed but changes with the water saturation within it.

Based on the two assumptions, Liu et al. (2005) proposed an ARM constitutive relation between the fraction of the active region and soil water saturation within it. The ARM constitutive relation is expressed as (Liu et al. 2005):

$$f = \left(S_e^*\right)^{\gamma} \tag{1}$$

Here *f* is the portion of the active region; γ is the ARM parameter that is a function of the fractal dimension of flow pattern and used to characterize the heterogeneity of the preferential flow pattern; S_e^* is the effective soil saturation of the whole domain and is calculated as:

$$S_e^* = fS_a \tag{2}$$

in which S_a is the effective water saturation of the active region and defined by

$$S_a = \frac{\theta_a - \theta_r}{\theta_s - \theta_r} \tag{3}$$

where θ_a is the water content of the active region; θ_s is the saturated water content; and θ_r is the residual water content. The parameters of θ_s and θ_r for the active and inactive regions are assumed to be the same during the infiltration process. From Eqs. (1) and (2), we obtain

$$f = (S_a)^{\frac{\gamma}{1-\gamma}} \tag{4}$$

After the fraction of the active region and water content in the region are measured, the ARM parameter (γ) can be determined using Eq. (1) or (4). The parameter γ is a positive value between zero and one and increases with the flow heterogeneity (Liu et al. 2005; Sheng et al. 2009). According to Liu et al. (2005), the

ARM parameter can be expressed as a function of the fractal dimension of the flow region as follows:

$$\gamma = 1 - \left(\frac{d_f}{D} \right)^{n^*}$$

(5)

where d_f is the fractal dimension of the preferential flow pattern; D is the Euclidean (topological) dimension of a space; n^* is a given iteration level.

Governing equations for water flow and solute transport

The governing equations for soil water flow and solute transport were derived based on the mass conservation principles and the basic concept of the ARM. By using the horizontally averaged soil water content (Liu et al. 2005; Sheng et al. 2009), it is assumed that the soil water and solute move in the z-direction only (Fig. 1). We derived the following governing equations for soil water flow (Eq. 6) and solute transport (Eq. 7):

$$-\frac{\partial}{\partial z}\left[fK_a\left(\frac{\partial h_a}{\partial z} + 1 \right) \right] + \frac{\partial (f\theta_a)}{\partial t} - \theta_i \frac{\partial f}{\partial t} + fr_{aw} = 0$$

(6)

$$-\frac{\partial}{\partial z}\left(f\theta_a D_a \frac{\partial c_a}{\partial z} \right) + \frac{\partial (fq_a c_a)}{\partial z} + \frac{\partial (f\theta_a c_a)}{\partial t} + \frac{\partial (f\rho_b s_a)}{\partial t} - (\theta_i c_i + \rho_b s_i)\frac{\partial f}{\partial t} + fr_{aw} c_{as} = 0$$

(7)

Here z is the vertical coordinate (upward positive); K_a and h_a are the unsaturated hydraulic conductivity and the pressure head of the active region; t is time; θ_i is the soil water content of the inactive region; r_{aw} is the sink term of soil water of the active region; D_a is the dispersion-diffusion coefficient of the active region; q_a (flow per unit area per unit time) is the vertical water flux within the active region; c_a and c_i (mass of solute per volume of soil solution) are the dissolved solute concentration in the active and inactive regions, respectively; s_a and s_i (mass of sorbent per mass of dry soil) are the absorbed solute concentrations in the active and inactive regions, respectively; ρ_b is the soil bulk density; c_{as} is the concentration of the sink term of soil water of the active region. More details about the derivation of the governing equations were provided in appendixes A and B. As Liu et al. (2005) and Sheng et al. (2009) have verified the constitutive relation of ARM (i.e. Eqs. (1) or (4)), the relation is directly coupled with the ARM governing equations.

By taking the portion of the preferential flow region (active region) (f) as a constant, the governing equations for soil water flow and solute transport are rewrote as follows:

$$-\frac{\partial}{\partial z}\left[K_a\left(\frac{\partial h_a}{\partial z}+1\right)\right]+\frac{\partial \theta_a}{\partial t}-r_{aw}=0 \tag{8}$$

$$-\frac{\partial}{\partial z}\left(\theta_a D_a \frac{\partial c_a}{\partial z}\right)+\frac{\partial (q_a c_a)}{\partial z}+\frac{\partial (\theta_a c_a)}{\partial t}+\frac{\partial (\rho_b s_a)}{\partial t}-r_{aw}c_{as}=0$$

(9)

Eqs. (8) and (9) are the classical mobile-immobile region models (MIM) for soil water flow and solute transport, respectively. In this study, for simplification, the exchanges of soil water and solute between the active (mobile) and inactive (immobile) regions were not considered in the ARM and the MIM. The essential difference between the ARM and the MIM is the treatments for the flow region. In the ARM, the preferential flow region changes with the flow and transport processes, while in the MIM the flow region is fixed during the processes.

Mathematically the ARM (Eqs. (6) and (7)) and the MIM (Eqs. (8) and (9)) are similar to the traditional continuum models for soil water flow and solute transport. In the traditional continuum models, it is assumed that water flow and solute transport occur in the whole domain (or single domain) of the unsaturated soil (or f = 1). Therefore, numerical programs of the traditional continuum models for the single continuum model can be easily modified to simulate flow and transport using the ARM and MIM. In this study, the numerical program of the traditional continuum models, SWMS_2D (Šimůnek et al. 1994), was modified for modeling preferential flow and transport in the soil using the ARM and the MIM.

A well-known statistical measure, the model efficiency (*ME*) (Loague and Green 1991; Nash and Sutcliffe 1970), is used to evaluate the performance of the ARM and

the MIM under the same conditions. The modeling efficiency is given as (Nash and Sutcliffe 1970)

$$ME = \frac{\sum_{1}^{N}(O-\overline{O})^2 - \sum_{1}^{N}(P-O)^2}{\sum_{1}^{N}(O-\overline{O})^2} \quad (10)$$

where O and P are the observed and predicted (simulated) values, respectively; $\overline{O}$ is the mean of the observed values. The maximum and ideal value for ME is 1.0, indicating that model predictions match the measured data exactly, while a negative value of ME indicates that model predictions are worse than using the observed mean as an estimate of the measured data (Larsson et al. 1999).

Field experiment

Experimental area description

A dye infiltration experiment was conducted in a sand soil in the Arid Land Research Center (35°32'N, 134°13'E), Tottori University, Japan, in 2004. The natural groundwater table was deeper than 5 m. Before the experiment, the upper 30 cm soil layer was tilled. After tillage, the soil was relatively homogeneous and no structural pores were observed in the whole infiltration depth. Before starting the infiltration process, a trench was manually dug to a depth of 1.5 m and 1.0 m apart from the experimental plot. Along the profile of the trench, soil samples (100 cm^3 for each)

were collected at the depths of 0-10, 10-20, 20-50, and 50-100 cm to measure soil properties in the lab, including the soil texture, bulk density, porosity, and saturated hydraulic conductivity (Dane and Topp 2004). The soil properties are summarized in Table 1.

Dye solution preparation

Brilliant Blue FCF solution with a concentration of 4 g/L (Flury and Flühler 1994) was prepared as the staining indication. Since the soil is sandy in the whole infiltration depth (Table 1), adsorption and retardation of the dye were expected to be extremely low (Flury and Flühler 1994; Lipsius and Mooney 2006) and the Brilliant Blue FCF was well suitable for visualizing flow patterns (Kasteel et al. 2002). To study the solute transport behavior, potassium chloride (KCl) was added to the Brilliant Blue FCF solution with a Cl^- concentration of 4 g/L (Flury and Wai 2003).

Experimental design

The experimental site was leveled to ensure a uniform surface condition and a micro sprinkler irrigation system was used for the experiment (Fig. 2a). The experiment area was about 4.0×3.0 m^2. At the beginning of experiment, the mixed solution was sprayed out on the soil surface with a constant rate of 0.015 mm/s for 40 min.

The measured water application uniformity was 90.2%. After irrigation, the experimental area was covered to prevent evaporation and left for 24 h to complete the infiltration process.

After 24 h of the dye solution applied, vertical soil profiles (Fig. 2a) were excavated across the experimental area (along the X-direction as showed in Fig. 2a) at a horizontal interval of 10 cm. After each profile was exposed, the surface was leveled and cleaned with a brush to remove soil particles resulted from digging. Staining patterns were recorded during day time using a CCD digital camera, with a piece of white sheet to diffuse the light and to avoid direct radiation. Before taking photos, the four edge points of a profile were marked. Then the photos of stained patterns were corrected for geometric distortion based on the edge points using the method by Forrer et al. (2000). Each pixel in the color images was classified as "stained" or "unstained" based on its red, green, and blue values following the procedure of Forrer et al. (2000). Each pixel represented 1×1 mm^2 of the original soil profile.

After the visualization process, soil samples were collected along each profile at the depths of 0, 10, 20, 30, 40, 50, 60, 80, and 100 cm and with a horizontal interval of 50 cm (Fig. 2a). At each distinct fingering path, soil samples were collected at the horizontal and vertical intervals of 5 cm (Fig. 2b). Soil water contents were

measured from the collected samples using the gravimetric method (Gardner 1986); Cl^- concentrations were determined from measurements of the electrical conductivities of the diluted soil solutions (1:5) (Rhoades 1982) with a CM 40G EC meter in the lab. Similar to the study of Öhrström et al. (2004), the effect of Brilliant Blue dye on electrical conductivity was ignored in our case. Furthermore, compared to the electric conductivities (EC) tested in the dye stained region, the ECs tested in the non-stained region were rather small (0.9 - 11.4% of the dye stained region). Therefore, the initial Cl^- concentration was set to be 0 in the whole infiltrated soil layer and the Cl^- concentrations of the dye stained region were estimated directly from the measured EC values. As the climate was arid and the soil was almost pure sand, it was assumed that the initial soil water contents within the stained and unstained regions were not significantly different after long-time soil water redistribution (Sheng et al. 2009). In addition, the upper 30 cm soil layer was tilled before experiment, which uniformed the initial soil water contents between the stained and unstained regions and changed the preferential flow paths between the upper and deeper soil layers. Undisturbed soil core samples were collected within the profiles at X = 0, 150, and 300 cm and the depths of 0, 20, 50, and 100 cm in each profile to measure the soil water retention curve in the lab (Klute 1986).

Determination of the hydraulic and transport parameters

As indicated in Table 1, the soil textures of different infiltrated depths were almost the same. Therefore, we used the averaged values of the parameters at the whole infiltrated soil layer as the input values for modeling.

Twelve groups of the measured data of soil water content vs. suction were fitted to the van Genuchten soil water retention function (van Genuchten 1980). The fitted parameters of the soil retention function were θ_r = 0.015 cm^3/cm^3, θ_s = 0.394 cm^3/cm^3, n = 3.095, and α = 0.0195 1/cm. As shown in Fig. 3, the 12 groups of soil water content vs. suction data were similar. Therefore, the soil layers of the whole experimental site ($4.0 \times 3.0 \times 1.0$ m^3) were considered as one single material with one set of the parameters. Transport parameters of the diffusion coefficient (D_d = 0.00028 cm^2/min) of Cl^- in free water and the longitudinal dispersivity (D_L = 1.0 cm) were taken from de Vos et al. (2002) and Šimůnek et al. (1994), respectively.

Results and discussion

Determination of the ARM parameter γ

An example of dye coverage distributions is shown in Fig. 4 with the measured maximum infiltration depth of 93 cm. Figs. 5a and b show the distributions of soil water content and Cl^- concentration before and after infiltration, respectively. The

distributions of soil water content and Cl^- concentration after the infiltration were measured from the samples within the stained regions. The constitutive relation (Eq. (4)) describes a positively correlated function between the fraction of active region and the soil water content in the region. However, Figs. 4 and 5a show different trends between the distributions of dye coverage and soil water content of the stained region. Dye coverage decreases with the infiltration depth steadily (Fig. 4), while the soil water content of the stained region (Fig. 5a) increases with the infiltration depth first within the soil layer to a depth about 40 cm and then decreases with the depth from the maximum soil water content to the initial soil water content. The different distributions of dye coverage and soil water content of the stained region were attributable to the soil water redistribution within the upper soil layer during the experiment period, resulting in shrinkage of the active region over the layer. However, the dye-stained region could not shrink along with the active region, which means that only a portion of the dye-stained region acted as the active region in the upper 40 cm of soil layer. On the other hand, within the deeper soil layer (below 40 cm), the infiltration process was going on at the end of experiment, and the dye stained region coincided with the active region in this soil layer. Therefore, the ARM parameter (γ) was determined by fitting Eq. (4) with the data of soil water content and fraction of the dye-stained region within the soil layer below 40 cm.

The fitting result is shown in Fig. 6 with a fitted γ value of 0.459 ($R^2 = 0.963$). The relative root mean square error (*RRMSE*) analysis (Basile et al. 2006) indicated that the data from the soil layer below 40 cm matched the fitted result very well (*RRMSE* = 6.9%).

Simulation results

Based on the experimental setup and tested results, the simulation domain was set as a soil column of 120 cm. The atmospheric boundary condition was used for the upper boundary (Šimůnek et al. 1994) and the bottom boundary was set as the specific pressure head condition. The initial soil water content was taken from the initially measured soil water content distribution and the initial Cl^- concentrations were set to be 0. The averaged soil water content and Cl^- concentration distributions were simulated using the ARM with $\gamma = 0.459$ and the MIM, respectively. For the MIM, the fraction of the mobile region was set up according to the dye coverage distribution from the experiment. Simulated distributions of horizontally averaged soil-water content and Cl^- concentration of the active region (only for ARM), the dye stained region, and the whole flow region using ARM (Fig. 7a and b) and MIM (Fig. 8a and b) were compared to the experimental results. Note that the dye stained region may be the totally active or partially active regions for the ARM and is the

mobile region for the MIM.

Under the same infiltration conditions, the predicted maximum infiltration depth using the ARM was 86 cm, which was 93% of the measured maximum infiltration depth (Fig. 7a). The predicted maximum infiltration depth using the MIM was 77 cm, 83% of the measured maximum infiltration depth (Fig. 8a). The different predicted results were attributable to the different treatments of the flow region in the two models: the flow region (i.e. the active region) is variable and positively correlated with the soil water content within it in the ARM; the flow region (i.e. the mobile region) is fixed and keep unchanged during the flow process in the MIM. The changeable active region in the ARM resulted in higher soil water content and thus higher unsaturated hydraulic conductivity than those in the flow region of the MIM. Accordingly, in the ARM a higher hydraulic pressure gradient was also formed at the infiltration front than in the MIM. For a given infiltration flux, a larger value of γ corresponds to a smaller active region and generates a faster preferential flow pattern.

Fig. 7a also shows that the simulated distribution of soil water content of the active region deviates obviously from the measured distribution of soil water content of the stained region in the upper 40 cm soil layer (ME = -2.11). As the active region of the soil layer above 40 cm shrank after 24 h infiltration and was much smaller

than the dye stained region, the predicted soil water content in the active region differed from the measured results in the upper soil layer. However, within the soil layer below 40 cm, the simulated distribution of soil water content of the active region matched the measured distribution of soil water content of the stained region well (*ME* = 0.83). The result also supports that the active region only coincided with the stained region in the soil layer below 40 cm. Although the simulated distribution of soil water content of the active region deviated much from the measured distribution in the soil layer above 40 cm, the simulated distributions of soil water content of the stained region and of the whole region were rather similar to the measured results of soil water content of the stained region and of the whole region in the whole infiltrated soil layer (with *ME*s equal to 0.84 and 0.90, respectively), respectively. These results indicated that the ARM could well capture the major behavior of preferential soil water flow in the unsaturated soil, especially considering that the only required information is the ARM parameter (γ), which was directly determined from the field data.

Fig. 7b shows that the predicted distribution of Cl^- concentration of the active region deviate much from the measured Cl^- concentrations of the stained region in the upper 40 cm soil layer (*ME* = -18.69), whereas the predicted and measured results agree well in the soil layer deeper than 40 cm (*ME* = 0.80). Different from

the distribution of predicted soil water content of the active region (Fig. 7a), the predicted distribution of Cl^- concentration of the active region displayed a steadily decreasing trend with the infiltration depth. The result was due to the ARM assumption that the movement of soil water and solute only occurs in the changeable active region. As the active region decreased in the upper soil, the solute moved within a smaller region. Although some Cl^- transported to the deeper soil layer through mass flow and diffusion, this decreasing influence on the Cl^- concentration might be rather inappreciable compared to the increasing influence caused by the decreasing of the transport region (i.e. the active region). Fig. 7b also shows that the predicted distributions of Cl^- concentration in the stained region and the whole region agree with the measured distributions well (with *ME*s equal to 0.83 and 0.88, respectively). These results indicate that the ARM can well capture the major behavior of preferential solute transport in the unsaturated soil.

Compared to the predictions from the ARM, the predicted soil water content and Cl^- concentration of the dye stained region (i.e. mobile region) and whole flow region using the MIM deviated significantly from the measured results (Figs. 8a and b). The *ME*s were 0.38 and 0.26 for predictions of the soil water content in the dye stained region and whole region, respectively. The *ME*s were -0.20 and 0.30 for predictions of Cl^- concentration in the dye stained region and whole region,

respectively. As the fraction of the flow region is a variable in reality (Larsson et al. 1999; van Dam et al. 1996), it is expected that the ARM provides more accurate predictions than the MIM.

Note that the ARM was developed for describing the macroscopic flow behavior, rather than detailed flow patterns in the unsaturated soil (Liu et al. 2005). Therefore, the ARM cannot be applied to describe the detailed soil water and solute distributions in the simulation domain. Nevertheless, given the mathematical simplicity of the ARM and the complexity of the flow patterns, the consistency of the holistic behavior (distributions of horizontally averaged soil water content and solute concentration) between the ARM predictions and the observations is remarkable. The horizontally averaged flow and transport behavior may be of most interest for practical soil contamination problems.

Results from this study also suggest that the ARM can be further improved by (1) more accurately considering mass transfer between the active and inactive regions and (2) relaxing the assumption that inactive region is completely immobile. More research is needed along these lines.

Summary and conclusions

Based on the concept of the ARM, new governing equations were derived for

modeling of preferential water flow and solute transport in the unsaturated soil. A field dye infiltration experiment was conducted to evaluate the governing equations for predicting the distributions of soil water content and solute concentration under the preferential flow process.

Distributions of the measured soil water content and fraction of the dye stained region indicated that the dye stained region was not coincident with the active region in the whole infiltrated soil layer of the field experiment. As the active region may shrink and be smaller than the dye stained region in the upper soil layer, not all the data from the whole soil layer should be used to fit the ARM parameter (γ). For this experimental data set, γ was estimated using the data of soil water content and fraction of the dye stained region from the soil layer below 40 cm.

Simulated distributions of soil water content and Cl^- concentration of the active region (only for ARM), the dye stained region, and the whole region using the ARM and the MIM were compared with the experimental data. The performances of the ARM and MIM were evaluated using the modeling efficiency (*ME*). The *ME* results showed that the ARM was able to capture the macroscopic (horizontally averaged) behavior of the preferential flow and transport, whereas the MIM did not provide reasonable predictions of the processes. Therefore, the ARM is a valuable improvement over the MIM. The ARM can be further improved by more accurately

considering mass transfer between the active and inactive regions and relaxing the assumption that inactive region is completely immobile.

Acknowledgements This research was financially supported in part by grants of the National Science Foundation of China (Nos. 50779080, 50528910, and 50579079) and the 973 Project, the National Basic Research Program of China (No. 2006CB403404). This work was also partially supported by the U.S. Department of Energy and LBNL under Contract No. DE-AC02-05CH11231.

Appendix A. Derivation of the governing equation for water flow

Fig. 1 schematically shows the vertical water flow occurring in a rectangular soil unit volume. Because the horizontally averaged soil water content is used in the ARM (Liu et al. 2005; Sheng et al. 2009), it is assumed that the soil water flows in the z-direction only. According to the mass conservation principle, we obtain the water conservation equation for the system during an arbitrary small time period Δt between t and $t + \Delta t$ as

$$V_{in} = V_{out} + V_{inc} + V_{sk} \tag{11}$$

Here V_{in} is the water volume flowing into the soil volume during Δt; V_{out} is the water volume flowing out from the soil volume during Δt; V_{inc} is the increase of the water volume stored in the soil volume during Δt; V_{sk} is the water volume extracted (e.g. plant root, positive) or supplied (e.g. irrigation, negative) from other processes during Δt.

For the one-dimensional vertical flow, the water volume flowing into the soil volume during Δt can be expressed as

$$V_{in} = q_a\left(x, z, t + \frac{1}{2}\Delta t\right) f\left(x, z, t + \frac{1}{2}\Delta t\right) \Delta x \Delta t \tag{12}$$

where q_a (flow per unit area per unit time) is the water flux within the active region in the *z*-direction (upward positive).

Similarly, the water volume flowing out from the soil volume during Δt is expressed as

$$V_{out} = q_a\left(x, z + \Delta z, t + \frac{1}{2}\Delta t\right) f\left(x, z + \Delta z, t + \frac{1}{2}\Delta t\right) \Delta x \Delta t \tag{13}$$

The increase of the water volume stored in the soil volume during Δt is expressed by

$$V_{inc} = \theta_a\left(x, z+\frac{1}{2}\Delta z, t+\Delta t\right) f\left(x, z+\frac{1}{2}\Delta z, t+\Delta t\right)\Delta x\Delta z$$
$$-\theta_a\left(x, z+\frac{1}{2}\Delta z, t\right) f\left(x, z+\frac{1}{2}\Delta z, t\right)\Delta x\Delta z$$
$$-\theta_i\left[f\left(x, z+\frac{1}{2}\Delta z, t+\Delta t\right) - f\left(x, z+\frac{1}{2}\Delta z, t\right)\right]\Delta x\Delta z$$

(14)

where θ_i is the soil water content within the inactive region.

The ARM assumes that water flow occurs in the active region exclusively. Therefore, it is assumed that the sink and source terms also appear in the active region only, and are expressed in the form of

$$V_{sk} = r_{aw}\left(x, z+\frac{1}{2}\Delta z, t+\frac{1}{2}\Delta t\right) f\left(x, z+\frac{1}{2}\Delta z, t+\frac{1}{2}\Delta t\right)\Delta x\Delta z\Delta t$$

(15)

where r_{aw} is the rates of water consumed and supplied in the active region of the soil volume.

Substituting Eqs. (12) to (15) into Eq. (11), dividing both sides by $\Delta x\Delta z\Delta t$, taking the limit, and rearranging the terms, we obtain (upward positive)

$$\frac{\partial(fq_a)}{\partial z} + \frac{\partial(f\theta_a)}{\partial t} - \theta_i\frac{\partial f}{\partial t} + fr_{aw} = 0$$

(16)

Equation (16) is the governing equation for water flow. Including Darcy's law in Eq. (16) yields

$$-\frac{\partial}{\partial z}\left[fK_a\left(\frac{\partial h_a}{\partial z}+1\right)\right] + \frac{\partial(f\theta_a)}{\partial t} - \theta_i\frac{\partial f}{\partial t} + fr_{aw} = 0$$

(17)

where K_a and h_a are the unsaturated hydraulic conductivity and the pressure head of the active region, respectively. The h_a and K_a can be expressed as the functions of θ_a (Liu et al. 2005; van Genuchten 1980):

$$h(S_a) = \frac{1}{\alpha}\left[(S_a)^{-1/m} - 1\right]^{1/n} = \frac{1}{\alpha}\left[\left(S_e^*\right)^{(\gamma-1)/m} - 1\right]^{1/n}$$

(18)

and

$$K_a = K_s S_a^{1/2}\left[1 - \left\{1 - S_a^{1/m}\right\}^m\right]^2 = K_s\left(S_e^*\right)^{(1-\gamma)/2}\left[1 - \left\{1 - \left(S_e^*\right)^{(1-\gamma)/m}\right\}^m\right]^2$$

(19)

where α (1/cm), n, and $m = 1 - 1/n$ are parameters; K_s is the saturated hydraulic conductivity of the active region.

Appendix B. Derivation of the governing equation for solute transport

Governing equation for solute transport is also derived using the procedure similar to the soil water flow. According to the mass conservation principle of solute transport, we have

$$M_{in} = M_{out} + M_{inc} + M_{sk}$$

(20)

where M_{in} is the solute mass transporting into the soil volume during Δt; M_{out} is the solute mass transporting out from the soil volume during Δt; M_{inc} is the increase of the solute mass stored in the soil volume during Δt; M_{sk} is mass of solute extracted (e.g. plant root, positive) or supplied (e.g. irrigation, negative) from other processes during Δt.

For the one-dimensional transport (upward positive), the solute mass transporting into the soil volume during Δt is expressed as

$$M_{in} = J_a\left(x, z, t + \frac{1}{2}\Delta t\right) f\left(x, z, t + \frac{1}{2}\Delta t\right) \Delta x \Delta t$$

(21)

where J_a (transport per unit area per unit time) is the solute flux within the active region in the *z*-direction, expressed as the sum of convection and dispersion/diffusion as follows

$$J_a = q_a c_a - \theta_a D_a \frac{\partial c_a}{\partial z}$$

(22)

in which c_a (mass of solute per volume of soil solution) is the dissolved solute concentration in the active region; D_a is the dispersion-diffusion coefficient of the active region.

Similarly, the solute mass leaving from the soil volume during Δt is expressed as

$$M_{out} = J_a\left(x, z+\Delta z, t+\frac{1}{2}\Delta t\right) f\left(x, z+\Delta z, t+\frac{1}{2}\Delta t\right)\Delta x\Delta t$$

(23)

The increase of the mass of solute stored in the soil volume during Δt can be expressed as

$$\begin{aligned} M_{inc} = {} & C_a\left(x, z+\frac{1}{2}\Delta z, t+\Delta t\right) f\left(x, z+\frac{1}{2}\Delta z, t+\Delta t\right)\Delta x\Delta z \\ & - C_a\left(x, z+\frac{1}{2}\Delta z, t\right) f\left(x, z+\frac{1}{2}\Delta z, t\right)\Delta x\Delta z \\ & - C_i\left[f\left(x, z+\frac{1}{2}\Delta z, t+\Delta t\right) - f\left(x, z+\frac{1}{2}\Delta z, t\right)\right]\Delta x\Delta z \end{aligned}$$

(24)

where C_a and C_i are the total concentrations of solute in all forms (including the solute dissolved in soil solution and soil gas, and adsorbed by soil particles) in the active and the inactive region, respectively. By assuming the solute only exists in the solid (absorbed by soil particles) and liquid (dissolved in the soil solution) phases, the terms C_a and C_i can be expressed as

$$C_a = \theta_a c_a + \rho_b s_a$$

(25)

and

$$C_i = \theta_i c_i + \rho_b s_i$$

(26)

where c_i (mass of solute per volume of soil solution) is the dissolved solute

concentration in the inactive region; s_a and s_i (mass of sorbent per mass of dry soil) are the absorbed solute concentrations in the active and inactive regions, respectively; ρ_b is the soil bulk density.

By assuming the sink and source term of solute occur in the active region exclusively, the solute mass extracted (sink, positive) and/or supplied (source, negative) from other processes is expressed as

$$M_{sk} = c_{as} r_{aw} \left(x, z + \frac{1}{2}\Delta z, t + \frac{1}{2}\Delta t \right) f \left(x, z + \frac{1}{2}\Delta z, t + \frac{1}{2}\Delta t \right) \Delta x \Delta z \Delta t \tag{27}$$

where c_{as} is the concentration of the sink term of soil water of the active region.

Substituting Eqs. (21) to (27) into Eq. (20), dividing the both sides by $\Delta x \Delta z \Delta t$, taking the limit, and rearranging the terms, we have (upward positive) the following governing equation for solute transport

$$-\frac{\partial}{\partial z}\left(f\theta_a D_a \frac{\partial c_a}{\partial z} \right) + \frac{\partial (f q_a c_a)}{\partial z} + \frac{\partial (f\theta_a c_a)}{\partial t} + \frac{\partial (f\rho_b s_a)}{\partial t} - (\theta_i c_i + \rho_b s_i)\frac{\partial f}{\partial t} + f r_{aw} c_{as} = 0 \tag{28}$$

References

Basile A, Coppola A, De Mascellis R, Randazzo L (2006) Scaling Approach to Deduce Field Unsaturated Hydraulic Properties and Behavior from Laboratory Measurements on Small Cores. Vadose Zone J 5: 1005–1016

Dane JH, Topp GC, editors (2004) Methods of soil analysis, Part 4 Physical methods. Madison, WI: Soil Sci Soc Am

de Vos JA, Raats PAC, Feddes RA (2002) Chloride transport in a recently reclaimed Dutch polder. J Hydrol 257: 59–77

Flury M, Flühler H (1995) Tracer characteristics of Brilliant Blue FCF. Soil Sci Soc Am J 59: 22–27

Flury M, Flühler H, Jury WA, Leuenberger J (1994) Susceptibility of soils to preferential flow of water: a field study. Water Resour Res 30: 1945–1954

Flury M, Flühler H (1994) Brilliant Blue FCF as a dye tracer for solute transport studies-A toxicological overview. J Environ Qual 23: 1108–1112

Flury M, Wai NN (2003) Dyes as tracers for vadose zone hydrology. Rev Geophys 41(1): 1002. doi:10.1029/2001RG000109

Forrer I, Parrita A, Kasteel R, Flühler H, Luca D (2000) Quantifying dye tracers in soil profiles by image processing. Eur J Soil Sci 51: 313–322

Gardner WH (1986) Water content. In: Klute A, editor. Methods of Soil Analysis, Part 1, Physical and Mineralogical Methods. Amer Soc of Agron, Madison, WI, pp 493–544

Gjettermann B, Nielsen KL, Petersen CT, Jensen HE, Hansen S (1997) Preferential flow in sandy loam soils as affected by irrigation intensity. Soil Technol 11:

139–152

Glass RJ (1993) Modeling Gravity-Driven fingering using modified percolation theory. In: Proceedings of the Fourth Annual International Conference on High Level Radioactive Waste Conference, Las Vegas, Nevada

Goulding KWT, Poulton PR, Webster CP, Howe MT (2000) Nitrate leaching from the Broadbalk Wheat Experiment, Rothamsted, UK, as influenced by fertiliser and manure inputs and the weather. Soil Use Manage 16: 244–250

Heppell CM, Burt TP, Williams RJ, Johnson AC (2000) A laboratory investigation of the release of a conservative tracer and herbicide from topsoil aggregates under varying rainfall intensities. Soil Use Manage 16: 175–182

Jarvis SC (2000) Progress in studies of nitrate leaching from grassland soils. Soil Use Manage 16: 152–156

Kasteel R, Vogel HJ, Roth K (2002) Effect of non-linear adsorption on the transport behavior of Brilliant blue in a field soil. Eur J Soil Sci 53: 231–240

Ketelsen H, Meyer-Windel S (1999) Adsorption of brilliant blue FCF by soils. Geoderma 90: 131–145

Klute A (1986) Water retention: Laboratory methods. In: Klute A, editor. Methods of Soil Analysis, Part 1 Physical and Mineralogical Methods. Amer Soc of Agron, Madison, WI, pp 635–662

Larsson MH, Jarvis NJ, Torstensson G, Kasteel R (1999) Quantifying the impact of preferential flow on solute transport to tile drains in a sandy field soil. J Hydrol 215: 116–134

Lipsius K, Mooney SJ (2006) Using image analysis of tracer staining to examine the infiltration patterns in a water repellent contaminated sandy soil. Geoderma 136: 865–875

Liu H, Doughty C, Bodvarsson GS (1998) An active fracture model for unsaturated flow and transport in fractured rocks. Water Resour Res 34: 2633–2646

Liu H, Zhang G, Bodvarsson GS (2003) The active fracture model: Its relation to fractal flow patterns and an evaluation using field observations. Vadose Zone J 2: 59–269

Liu H, Zhang R, Bodvarsson GS (2005) An active region model for capturing fractal flow patterns in unsaturated soils: Model development. J Contam Hydrol 80: 18–30

Loague K, Green RE (1991) Statistical and graphical methods for evaluating solute transport models: overview and application. J Contam Hydrol 7: 51–73

Morris C, Mooney SJ (2004) A high-resolution system for the quantification of preferential flow in undisturbed soil using observations of tracers. Geoderma 118: 133–143

Nash JE, Sutcliffe JE (1970) River flow forecasting through conceptual models. Part 1-A discussion of principles. J Hydrol 10: 282–290

Öhrström P, Hamed Y, Persson M, Berndtsson R (2004) Characterizing unsaturated solute transport by simultaneous use of dye and bromide. J Hydrol 289: 23–35

Öhrström P, Persson M, Albergel J, Zante P, Nasri S, Berndtsson R, Olsson J (2002) Field-scale variation of preferential flow as indicated from dye coverage. J Hydrol 257: 164–173

Persson M, Yasuda H, Albergel H, Berndtsson R, Zante P, Nasri S, Öhrström P (2001) Modeling plot scale dye penetration by a diffusion limited aggregation (DLA) model. J Hydrol 250: 98–105

Quisenberry VL, Phillips RE, Zeleznik JM (1994) Spatial distribution of water and chloride macropore flow in a wellstructured soil. Soil Sci Soc Am J 58: 1294–1300

Reichenberger S, Amelung W, Laabs V, Pinto A, Totsche KU, Zech W (2002) Pesticide displacement along preferential flow pathways in a Brazilian Oxisol. Geoderma 110: 63–86

Rhoades JD (1982) Soluble salts. In: Page AL, Miller RH, Keeney DR, editors. Methods of soil analysis, Part 2 Chemical and Microbiological Properties. Amer Soc of Agron, Madison, WI, pp 167–179

Sheng F, Wang K, Zhang R, Liu H (2009) Characterizing soil preferential flow using iodine–starch staining experiments and the active region model. J Hydrol 367: 115–124

Šimůnek J, Jarvis NJ, van Genuchten MTh, Gardenas A (2003) Review and comparison of models for describing non-equilibrium and preferential flow and transport in the vadose zone. J Hydrol 272: 14–35

Šimůnek J, Vogel T, van Genuchten MTh (1994) The SWMS_2D code for simulating water flow and solute transport in two-dimensional variably saturated media. Version 1.21, Research Report No. 132, US Salinity Laboratory, Riverside, CA

Smith JE, Zhang ZF (2001) Determining effective interfacial tension and predicting finger spacing for DNAPL penetration into water-saturated porous media. J Contam Hydrol 48: 167–183

van Dam JC, Wosten JHM, Nemes A (1996) Unsaturated soil water movement in hysteretic and water repellent field soils. J Hydrol 184: 153–173

van Genuchten MTh (1980) A closed-form equation for predicting the hydraulic conductivity of unsaturated soils. Soil Sci Soc Am J 44:892–898

van Genuchten MTh, Wierenga PJ (1976) Mass transfer studies in sorbing porous media. I. Analytical solutions. Soil Sci Soc Am J 40: 473–481

Wang K, Zhang R, Yasuda H (2006) Characterizing heterogeneity of soil water flow by dye infiltration experiments. J Hydrol 328: 559–571

Table 1 Soil physical and hydraulic properties.

Depth (cm)	Texture			Bulk density, ρ_b (g/cm^3)	Porosity (%)	Saturated hydraulic conductivity, K_s (cm/s)
	>50 μm (%)	2~50 μm (%)	<2 μm (%)			
0-10	100	0	0	1.45	40.2	6.44×10^{-4}
10-20	100	0	0	1.46	40.4	4.24×10^{-4}
20-50	100	0	0	1.48	39.2	3.76×10^{-4}
50-100	100	0	0	1.50	38.9	3.76×10^{-4}

Figure List

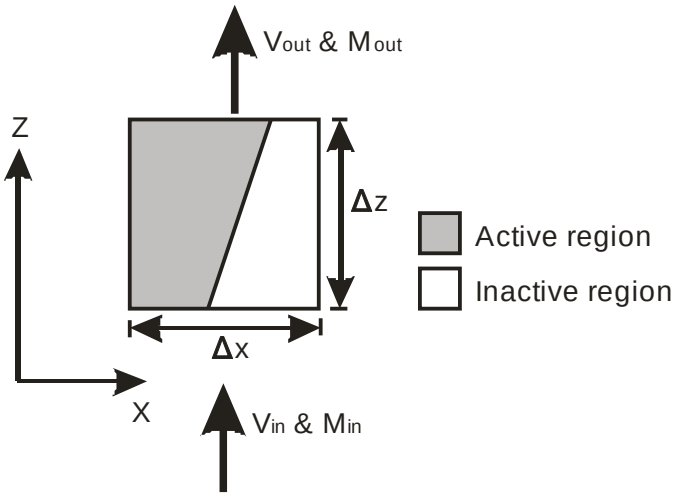

Figure 1

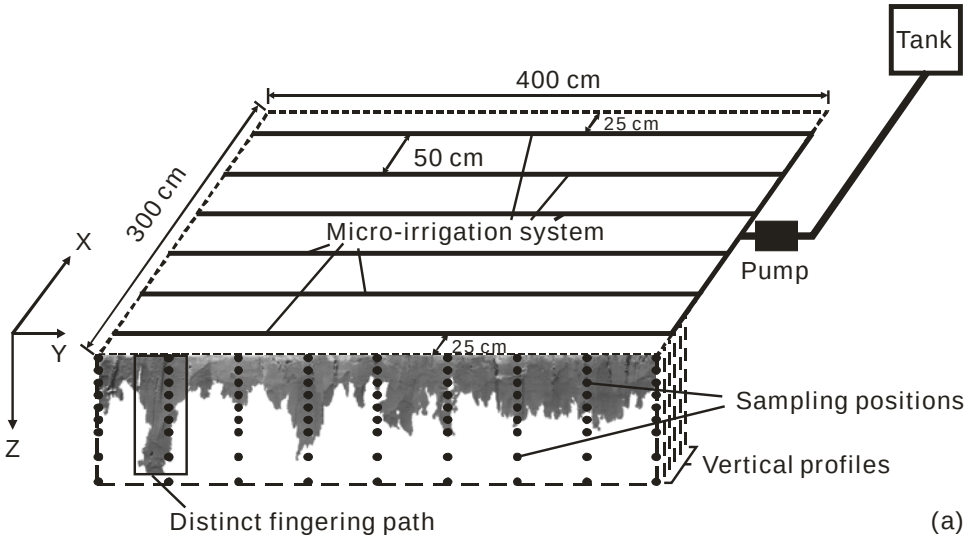
Tank
400 cm
25 cm
50 cm
300 cm
X
Micro-irrigation system
Pump
Y
25 cm
Sampling positions
Z
Vertical profiles
Distinct fingering path
(a)

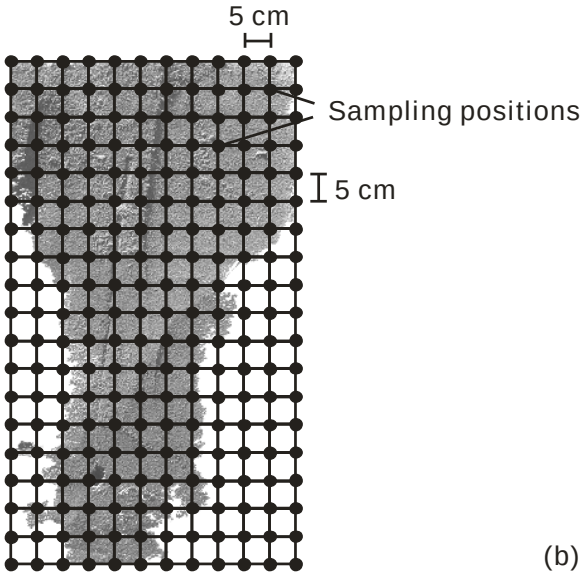
5 cm
Sampling positions
5 cm
(b)

Figure 2

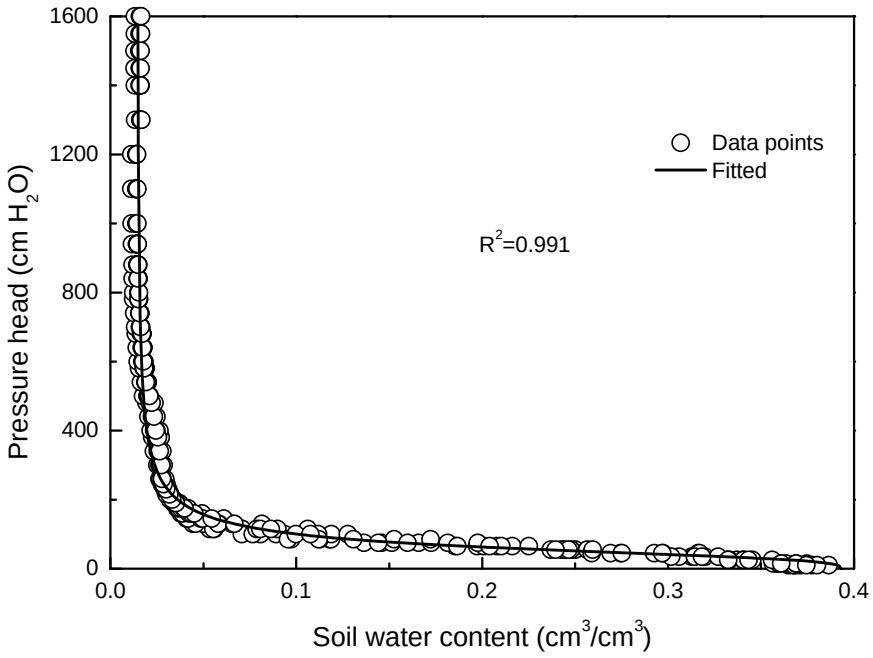
1600
1200
800
400
0
0.0
0.1
0.2
0.3
0.4
Pressure head (cm H2O)
Soil water content (cm3/cm3)
Data points
Fitted
R2=0.991

Figure 3

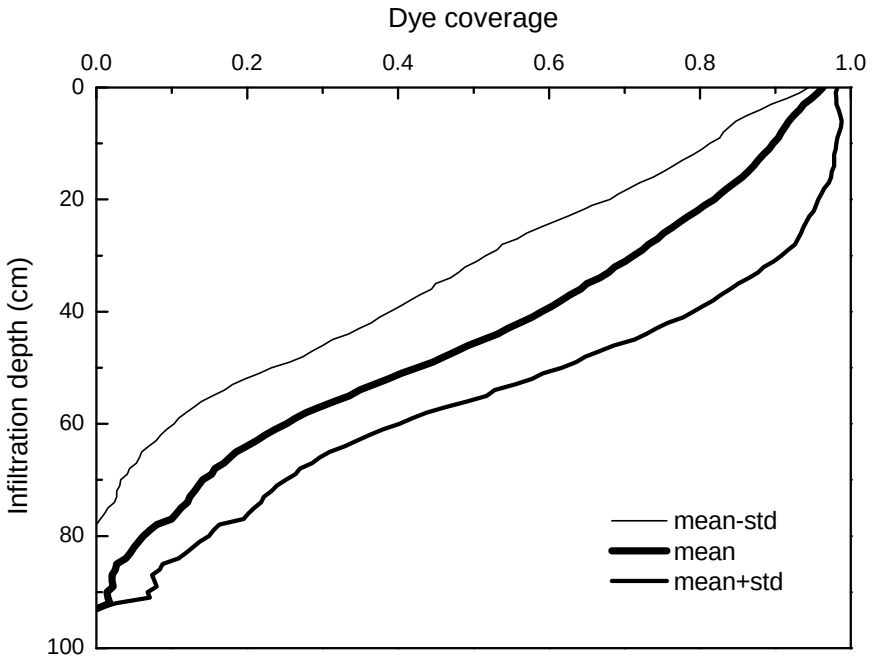
Dye coverage
0.0
0.2
0.4
0.6
0.8
1.0
0
20
40
60
80
100
Infiltration depth (cm)
mean-std
mean
mean+std

Figure 4

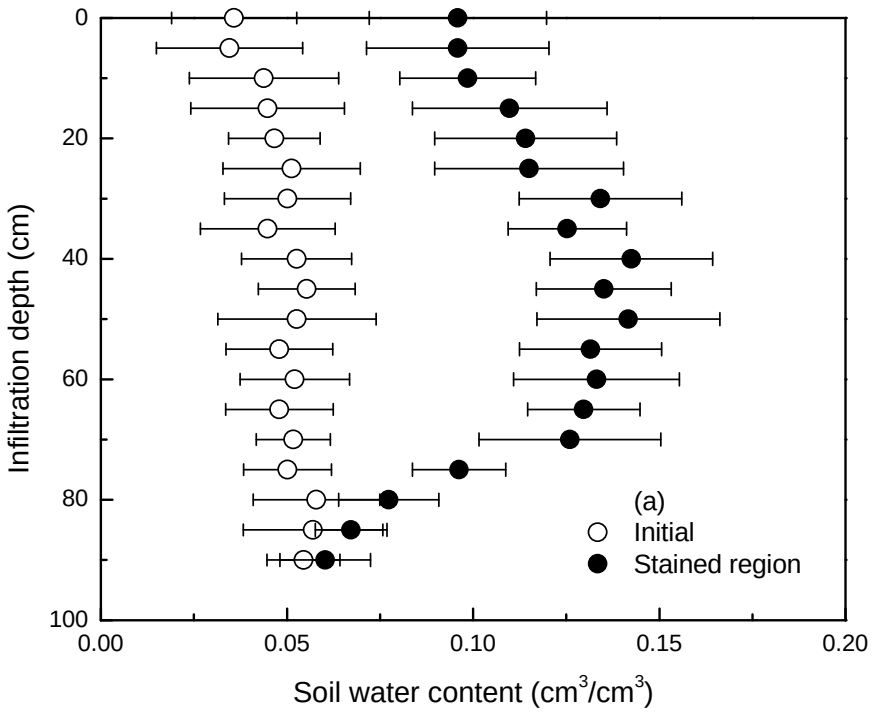
Infiltration depth (cm)
0
20
40
60
80
100
0.00
0.05
0.10
0.15
0.20
Soil water content (cm3/cm3)
(a)
Initial
Stained region

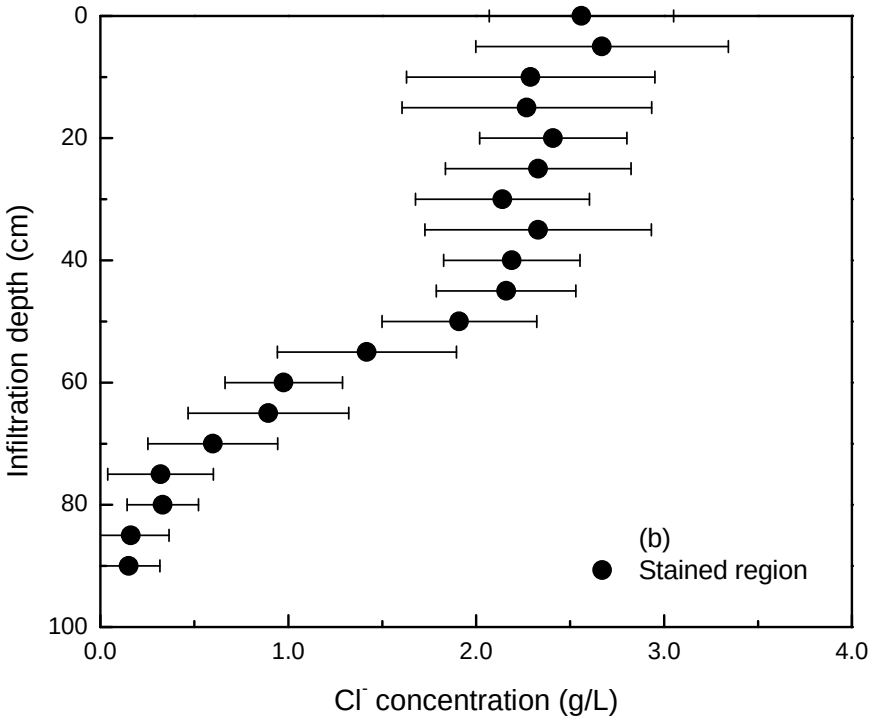
Infiltration depth (cm)
0
20
40
60
80
100
0.0
1.0
2.0
3.0
4.0
Cl- concentration (g/L)
(b)
Stained region

Figure 5

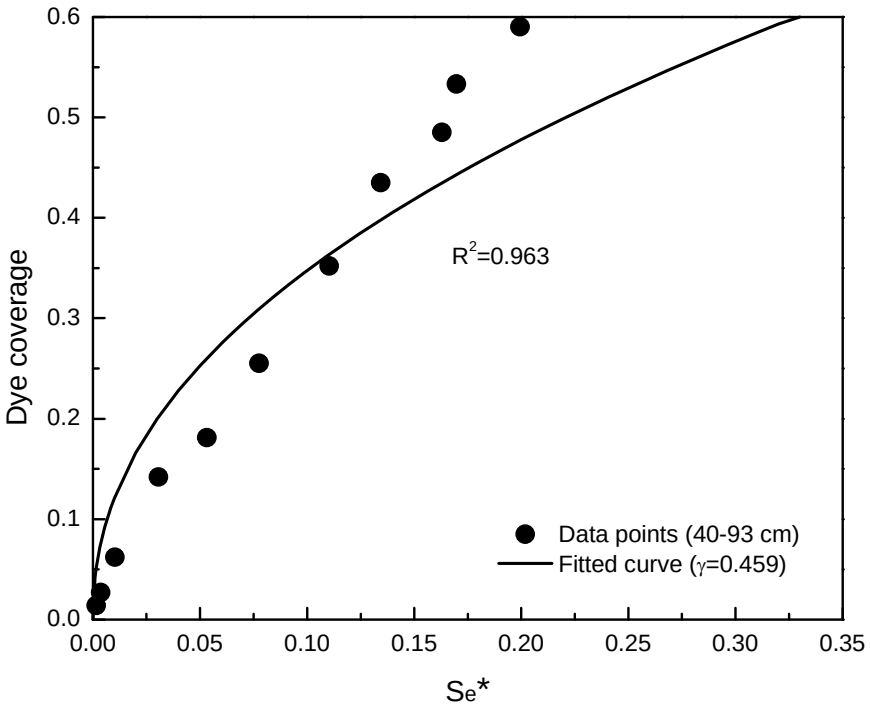
Dye coverage
Se*
R2=0.963
Data points (40-93 cm)
Fitted curve (γ=0.459)
0.0
0.1
0.2
0.3
0.4
0.5
0.6
0.00
0.05
0.10
0.15
0.20
0.25
0.30
0.35

Figure 6

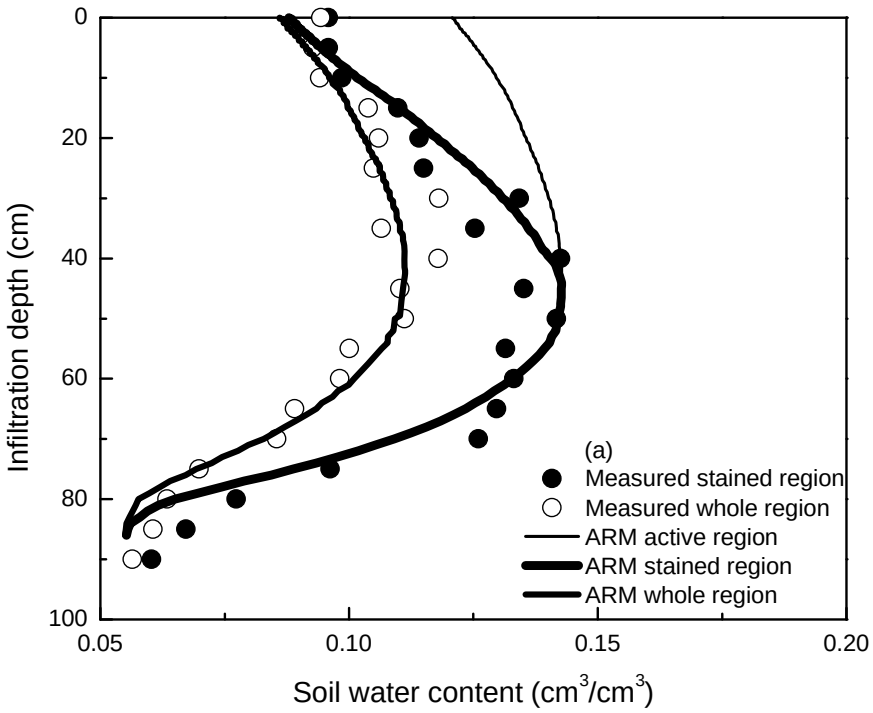
Infiltration depth (cm)
0
20
40
60
80
100
0.05
0.10
0.15
0.20
Soil water content (cm3/cm3)
(a)
Measured stained region
Measured whole region
ARM active region
ARM stained region
ARM whole region

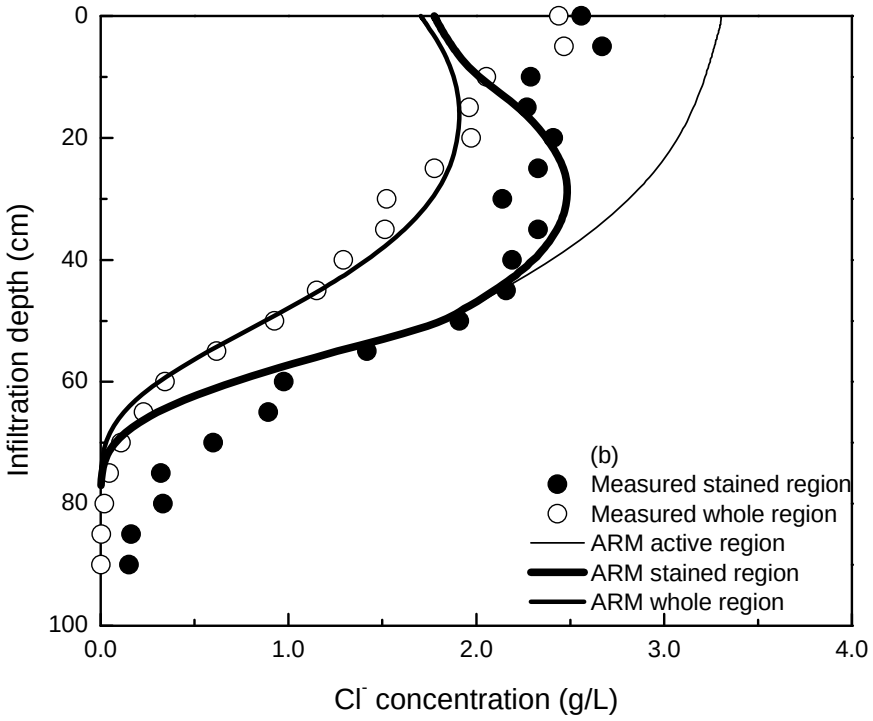
Infiltration depth (cm)
0
20
40
60
80
100
0.0
1.0
2.0
3.0
4.0
Cl- concentration (g/L)
(b)
Measured stained region
Measured whole region
ARM active region
ARM stained region
ARM whole region

Figure 7

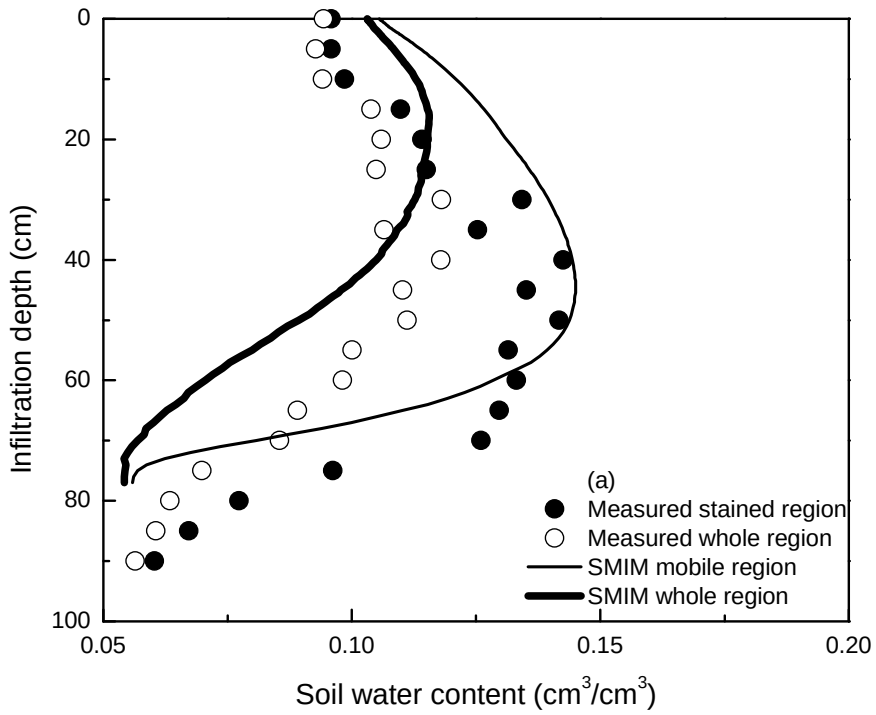
0
20
40
60
80
100
0.05
0.10
0.15
0.20
Infiltration depth (cm)
Soil water content (cm3/cm3)
(a)
Measured stained region
Measured whole region
SMIM mobile region
SMIM whole region

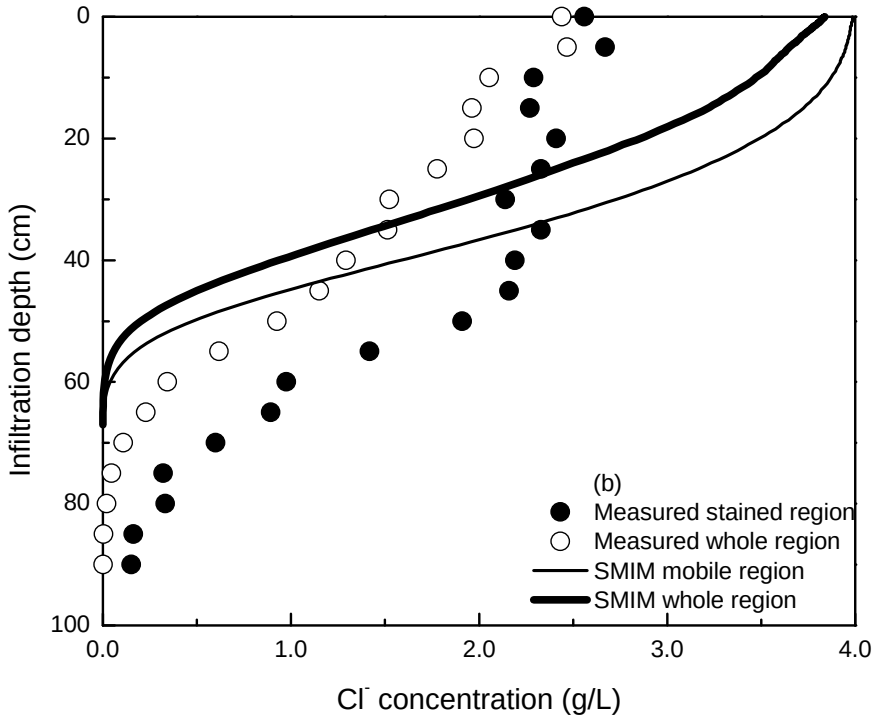
0
20
40
60
80
100
0.0
1.0
2.0
3.0
4.0
Infiltration depth (cm)
Cl- concentration (g/L)
(b)
Measured stained region
Measured whole region
SMIM mobile region
SMIM whole region

Figure 8